Electronic Supplementary Information for

Electrostatic induction promotes photocatalytic contaminant mineralization in saline wastewater

Shugong Gao,[a,c,#] Tingyun Ge,[a,c,#] Bo Li[*b] and Jiazang Chen[*a,c]

[a] State Key Laboratory of Coal Conversion, Institute of Coal Chemistry, Chinese Academy of Sciences, Taiyuan 030001, China

[b] Lanzhou Petrochemical Research Center, Petrochemical Research Institute, PetroChina, Lanzhou 730060, China

[c] Center of Materials Science and Optoelectronics Engineering, University of Chinese Academy of Sciences, Beijing 100049, China

Corresponding Authors

[*]Email: chenjiazang@sxicc.ac.cn (J.C.); libo931@petrochina.com.cn (B.L.)

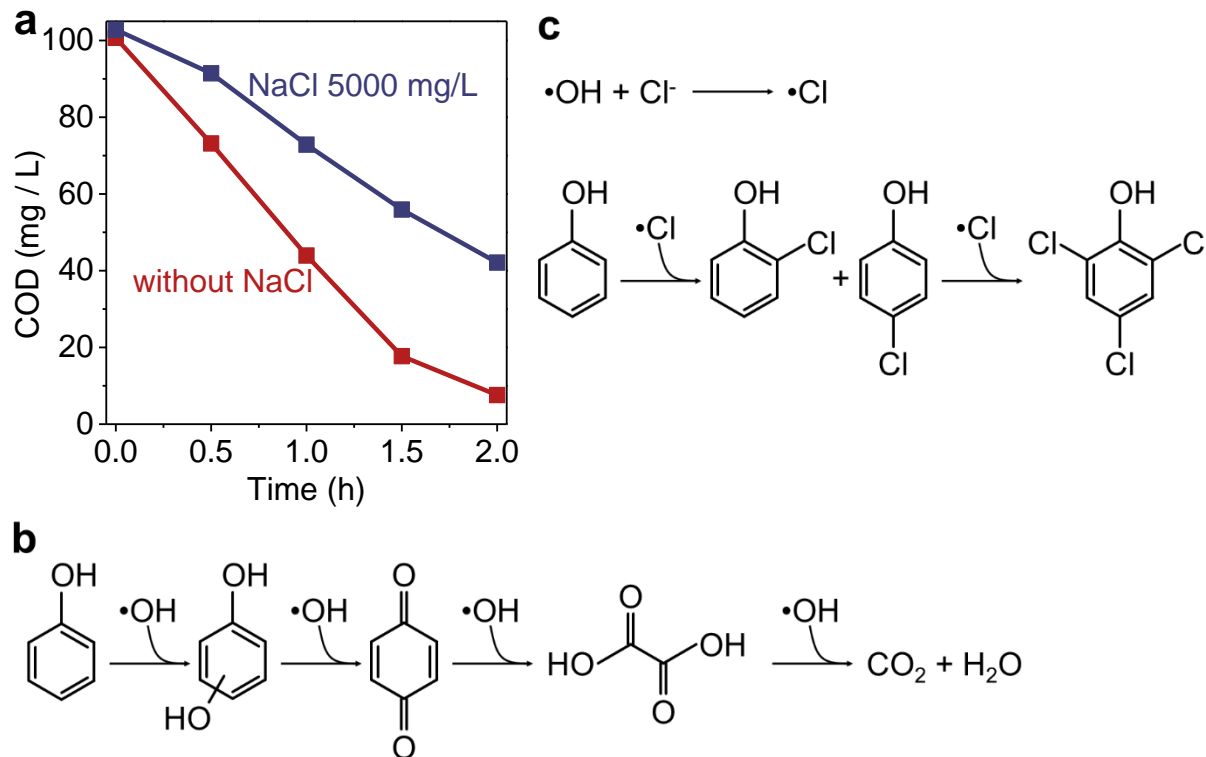Author Contributions

[#]These authors contributed equally.

Figure S1. The influence of salt (NaCl) on photocatalytic mineralization of phenol (42 mg/L, COD: ~100 mg/L) in 1 L wastewater over Pt/TiO_2 photocatalyst (a). The mineralization of phenol is efficient (a) by reacting with hydroxyl radicals according to the proposed route (b) without interference by salt.[1] By introducing NaCl (5000 mg/L) into the reaction system, phenol mineralization becomes less efficient (a). This should be ascribed to the fact that the introduced NaCl undesirably consumes hydroxyl radicals (•OH) by reaction with Cl^- (c).[2] Since the initial concentration of phenol (0.45 mM) is ~192 times lower than that (85.56 mM) of the NaCl in molar, the probability for collision of •OH with Cl^- can be much higher than that with contaminant. The oxidizing reactivity of the formed oxidized species like •Cl is lower than that of •OH and can hardly occur ring-opening reaction (c). The introduction of NaCl into the reaction system thus will slow the photocatalytic phenol mineralization (a).
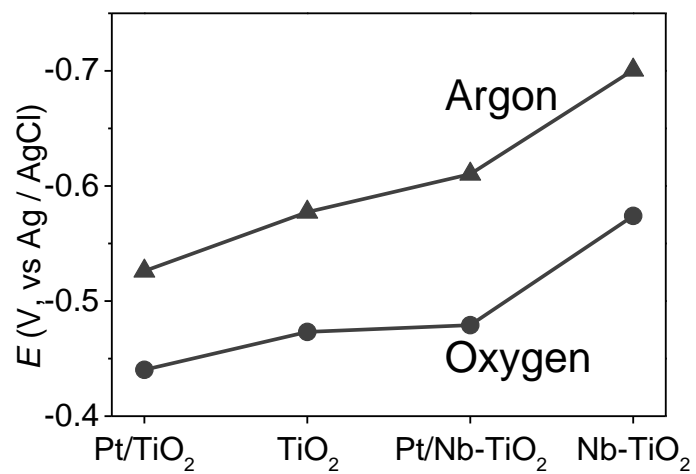
Figure S2. Photoinduced equilibrium potentials of TiO_2 and $Nb-TiO_2$ with and without loading platinum cocatalyst in argon and oxygen bubbled phosphate buffer solution.
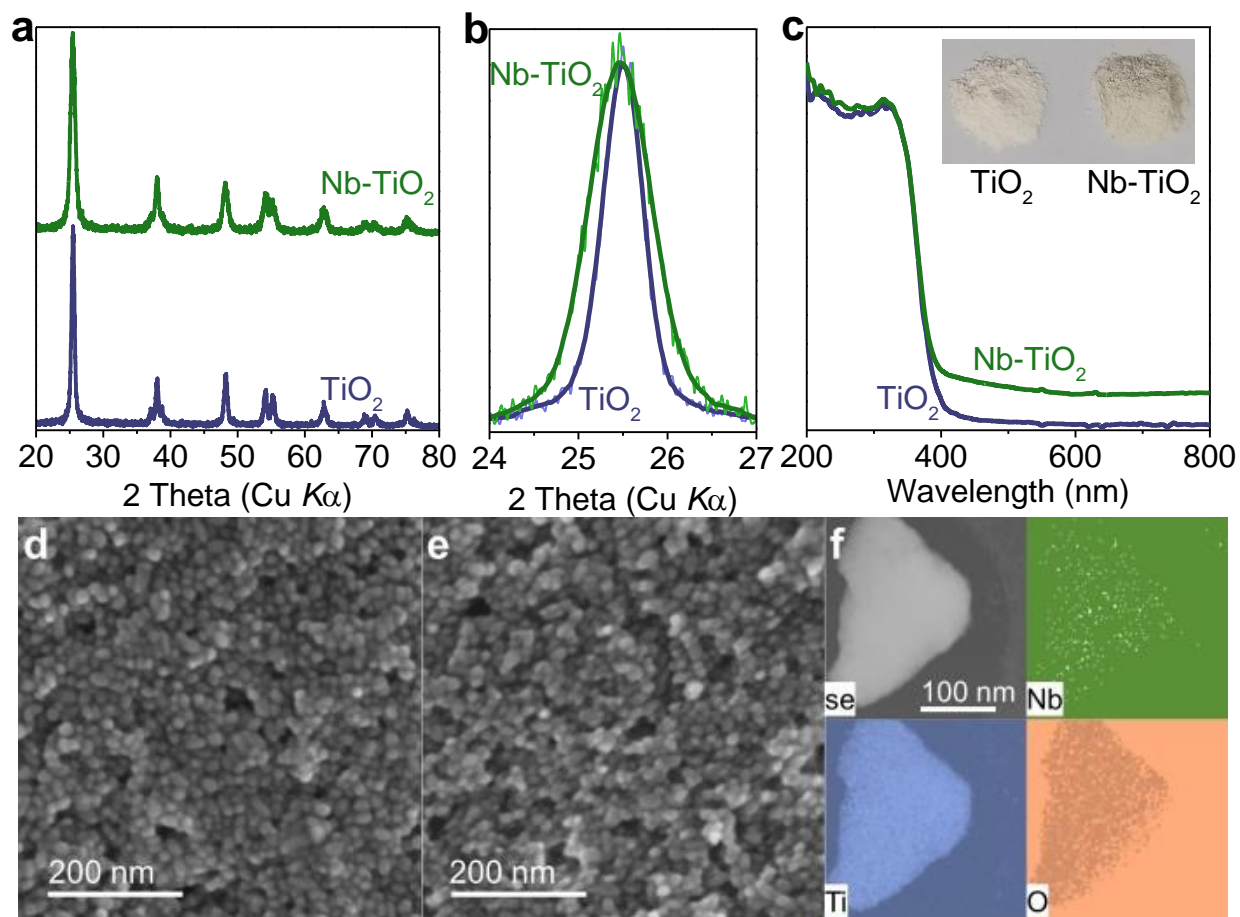
Figure S3. X-ray diffraction patterns (a, b), ultraviolet-visible absorption spectra (c), electron microscopy images (d, e), and high angle annular dark field electron microscopy and elementary mapping images (f) of TiO_2 (d) and $Nb-TiO_2$ (e, f). The digital images show that TiO_2 becomes grey after electronic doping (inset, c). This makes $Nb-TiO_2$ absorb visible light (c).
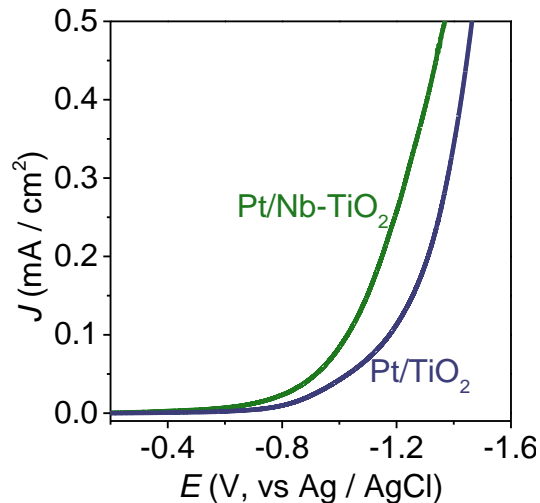
Figure S4. Voltammetry behaviors of Pt/TiO$_2$ and Pt/Nb-TiO$_2$ in phosphate buffer solution. The larger cathodic current indicates that the doping created electronic states play the role of intermediates for trap-assisted charge recombination. This makes the interfacial transfer of electrons from Nb-TiO$_2$ to platinum easy, as compared with that from TiO$_2$.
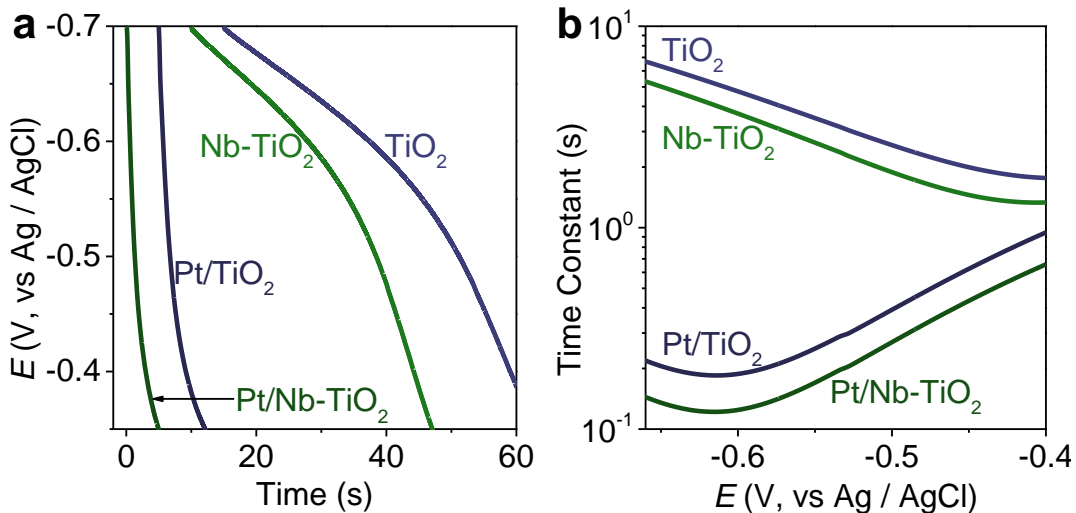

Figure S5. By monitoring the decay behaviors of open-circuit potential (a), we can obtain the time constants (b) for TiO$_2$ and Nb-TiO$_2$ electrodes with and without loading platinum cocatalyst.[3, 4] Prior to recording the decay, the electrodes were bias at -0.7 V (vs Ag/AgCl) in an argon saturated solution.
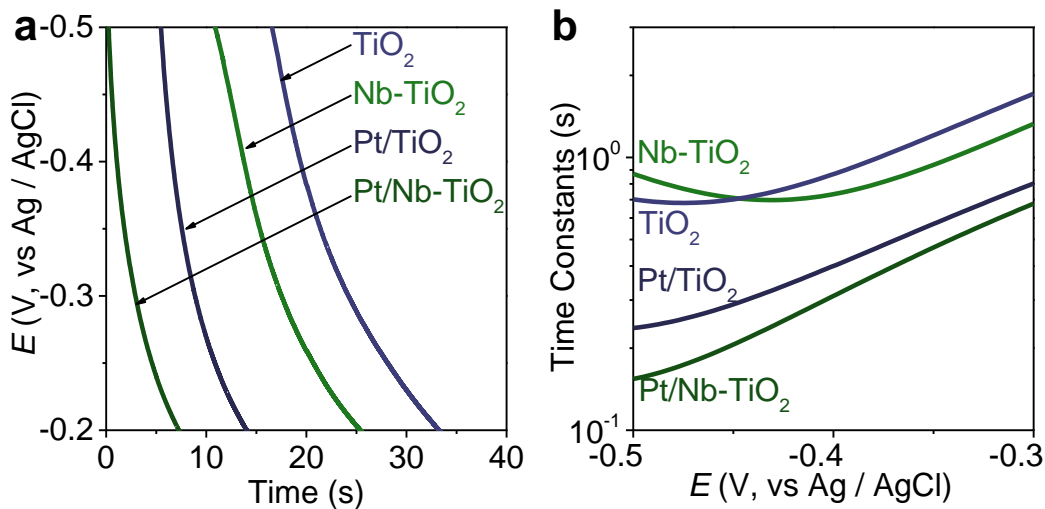
Figure S6. The open-circuit potential decay behaviors (a) and the obtained time constants (b) for

TiO$_2$, Nb-TiO$_2$, Pt/TiO$_2$, and Pt/Nb-TiO$_2$ electrodes in oxygen saturated solution.
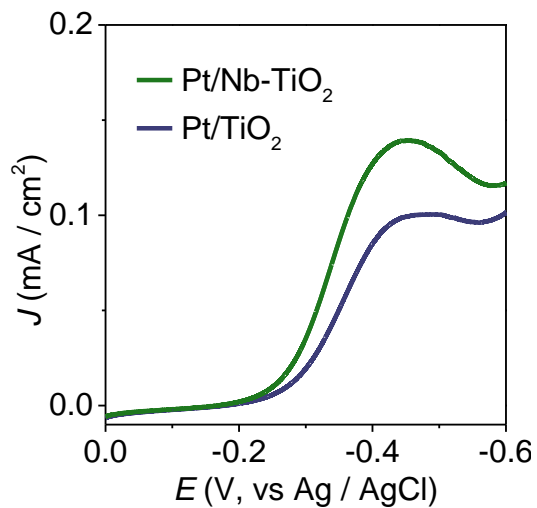

Figure S7. Oxygen reduction behaviors of Pt/TiO$_2$ and Pt/Nb-TiO$_2$. Since the electronic doping

can create intermediates for facilitating semiconductor-cocatalyst interfacial electron transfer by

trap-assisted charger recombination (Figures 3, S4, S5, S6), Pt/Nb-TiO$_2$ electrode exhibit higher

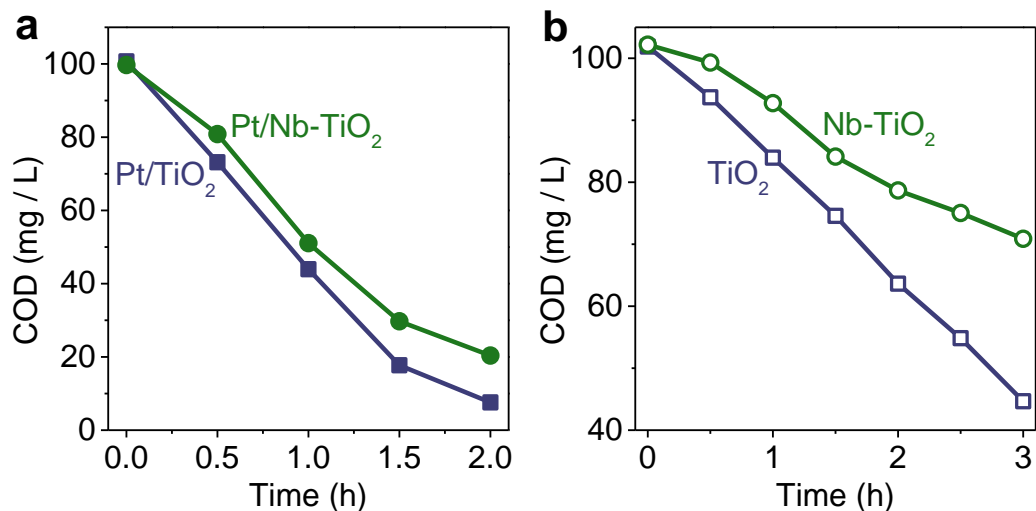cathodic current than that of Pt/TiO$_2$ for oxygen reduction.

Figure S8. Photocatalytic mineralization of phenol (42 mg/L, COD: ~100 mg/L) in 1 L salt-free wastewater over (Nb-)TiO$_2$ with (a) and without (b) loading platinum cocatalyst.
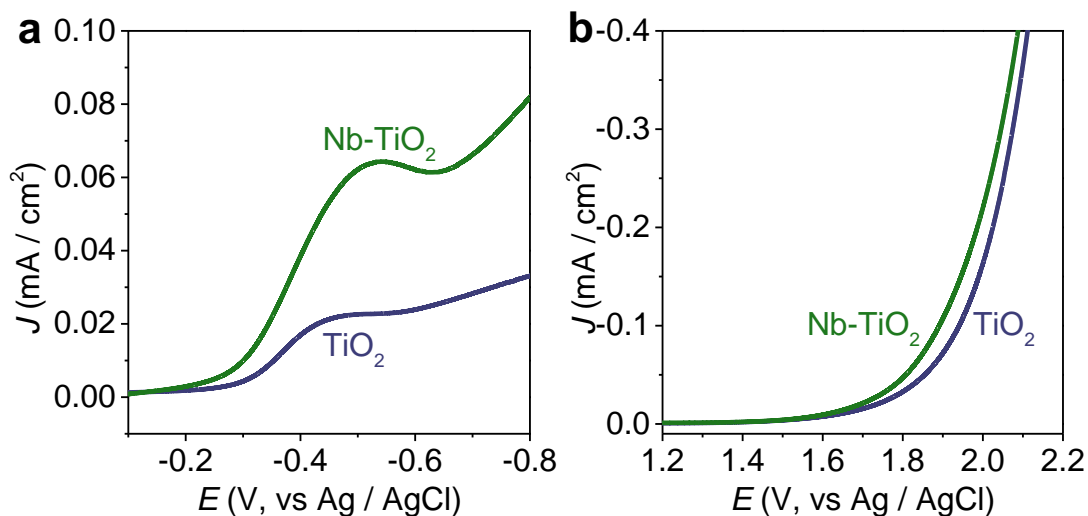
Figure S9. Oxygen reduction (a) and water oxidation (b) behaviors of TiO$_2$ and Nb-TiO$_2$ deposited on a rotated glassy carbon disk. The electronic doping that enriches the electronic cloud of the formed Nb-TiO$_2$ (Figure 2) can strengthen the adsorption of oxygen species.[5] This will increase both the cathodic (a) and anodic (b) currents for Nb-TiO$_2$. The negative shift of the onset potential for the anodic current (b) will undesirably reduce the generation rate of hydroxyl radicals (Figure S10).[6]
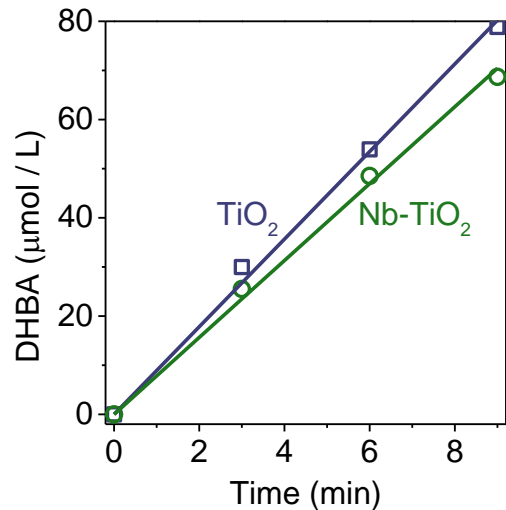
Figure S10. Photoinduced generation of hydroxyl radicals (•OH) over dispersed TiO_2 and Nb-TiO_2. The generated •OH can be captured by salicylic acid (•OH trapping agent). The generation rate of •OH can be determined by measuring the concentration of the formed dihydroxybenzoic acids (DHBA). By averaging the concentration of DHBA and correcting with trapping ratio,[7] the estimated generation rates of •OH over TiO_2 and Nb-TiO_2 are 0.27 and 0.23 mmol/h, respectively.

Figure S11. Influence of sodium ions on voltammetry behaviors of TiO_2 and $Nb-TiO_2$ in $LiClO_4$ aqueous solution. To eliminate the interference by the conductivity of solution, the concentrati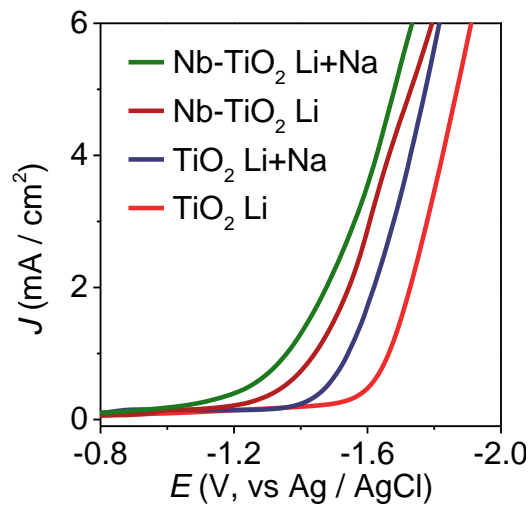ons of cations for the electrolyte with (0.1 M $NaClO_4$ + 0.4 M $LiClO_4$) and without (0.5 M $LiClO_4$) sodium ions are the same.
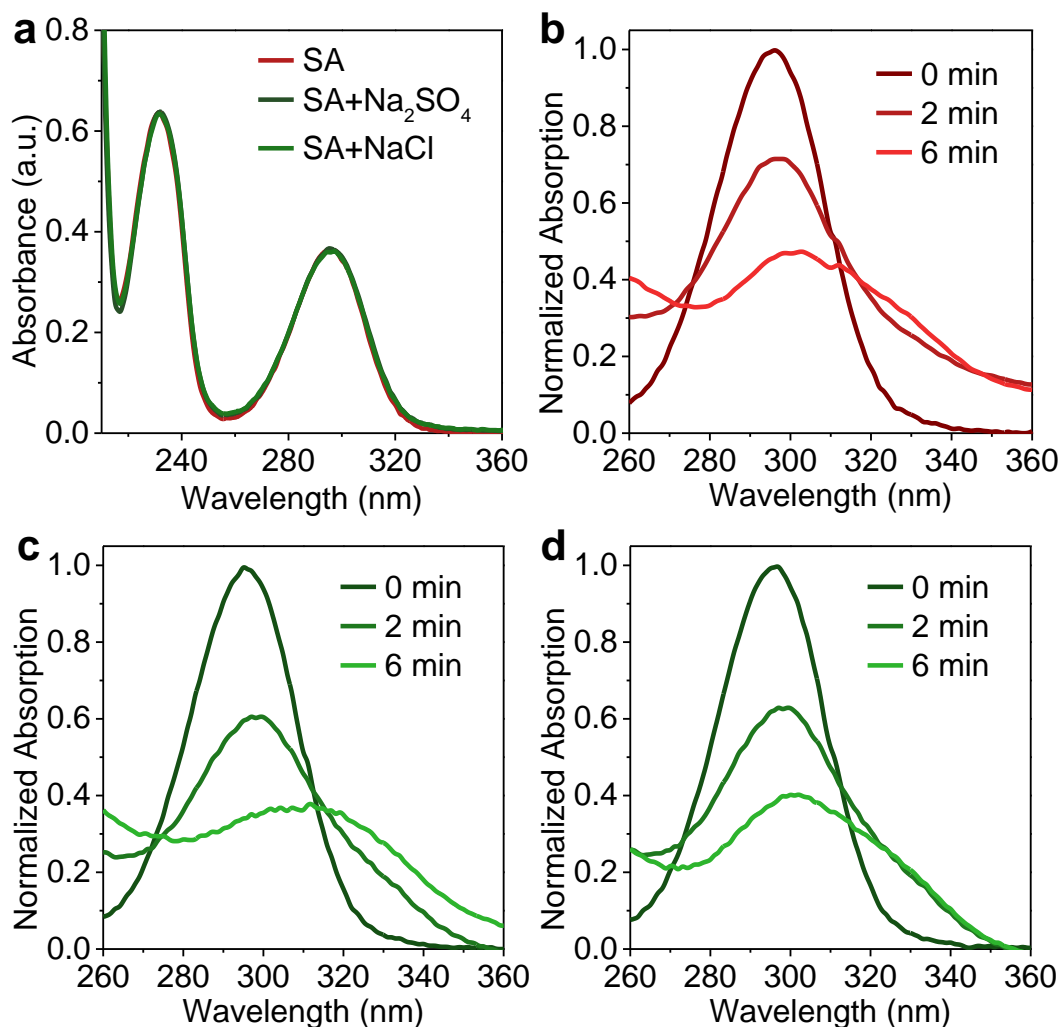
Figure S12. Influence of salt on light absorption of salicylic acid (SA) (a) and photoinduced generation of hydroxyl radicals ($\cdot$OH) over Nb-TiO$_2$ (b-d). The generation of $\cdot$OH can be reflected by the decreases in absorbance for SA (at ~296 nm) and the rise of the absorbance (in long wavelength region) that can be ascribed to the formed 2,3-dihidroxybenzoic acid (2,3-DHBA) and 2,5-dihidroxybenzoic acid (2,5-DHBA) with maximal absorbance respectively at ~310 and ~329 nm.[8] Compared with the case without salt (b), the rapid decay of SA absorbance indicates that the introduction of sodium ion by Na$_2$SO$_4$ facilitates $\cdot$OH generation (c). Similarly, the sodium ions introduced into the solution by NaCl can also facilitate $\cdot$OH generation (d).

Figure S13. Photocatalytic mineralization of phenol (42 mg/L, COD: ~100 mg/L) in 1 L saline and salt-free wastewater over TiO_2.
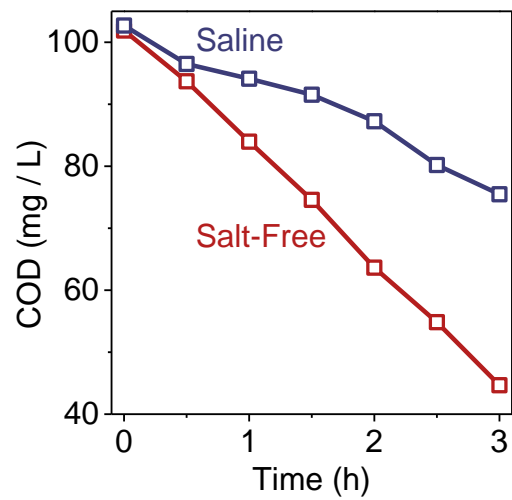
Experimental section

S1. Materials. Niobium-doped TiO_2 (Nb-TiO_2) can be synthesized by solvothermal treatment of titanium-containing precursors in the presence of $NbCl_5$. Briefly, 0.1586 g $NbCl_5$ was dissolved into 13.4 mL acetic acid under vigorously stirring for 2 h. Then, 20 mL tetrabutyl titanate were added into the dispersion. After stirring for 5 h, the dispersion was transferred to a sealed Teflon-lined autoclave that was heated at 220 ℃ for 12 h to grow nanoparticles. After reaction, Nb-TiO_2 was collected and washed with ethanol and water, and dried at 60 ˚C in vacuum overnight.

Loading platinum cocatalyst onto (Nb-)TiO_2 nanoparticles can be realized by photodeposition of platinum-containing precursor. Briefly, 0.2 g TiO_2 was dispersed into 200 mL methanol (20 %) aqueous solution containing 2 mg Pt (in H_2PtCl_6 precursor). Then, the dispersion that was bubbled with nitrogen was irradiated (300-W high-pressure Hg-lamp) for 90 min. After that, the precipitate was collected and washed with water and ethanol, and dried at 60 ˚C in vacuum overnight.

The morphologies of samples were characterized by scanning electron microscope (JSM-7900F). Powder X-ray diffraction patterns were recorded by a Bruker D8 Advanced diffractometer using Cu K_α irradiation. X-ray photoelectron spectroscopy measurements were carried out on an ThermoFisher EscaLab 250Xi emission using a monochromatic Al K_α source. UV-vis absorption spectra were recorded by performing a Shimadzu UV-3600 spectrometer.

S2. Semiconductor (Photo)Electrochemistry and Photochemistry. The electrochemical and photoelectrochemical measurements were conducted in tri-electrode systems, in which a piece of carbon cloth was used as counter electrodes, a liquid bridge containing an inert electrolyte (KCl) was used to connect the reference electrode (Ag/AgCl/Sat. KCl) and the cell. For most cases, 0.2 M phosphate buffer solution (PBS) was used as the electrolyte (Figures S2, S4, S5, S6, S7, S9).

(Nb-)TiO$_2$ electrode can be prepared by depositing the paste onto fluorine-doped tin oxide (FTO) conducting glass. The paste can be prepared by mixing 1 g (Nb-)TiO$_2$ into 10 mL anhydrous ethanol. After coating, (Nb-)TiO$_2$ electrodes can be obtained by heating the film at 500 °C for 60 min in air.

To investigate the (photo)electrochemical behaviors of Pt/(Nb-)TiO$_2$, a compact layer was deposited onto the FTO glass to avoid the possible contact of Pt to FTO. The compact layer can be formed by depositing 10 μL titanium-containing alcoholic solution (10 mL ethanol + 1.485 mL Triton X-100 + 2 mL acetic acid + 0.102 mL tetrabutyl titanate) onto FTO glass following with heat treatment at 500 °C for 60 min in air. After that, 20 μL Pt/(Nb-)TiO$_2$ dispersion (5 mg Pt/(Nb-)TiO$_2$ + 0.5 mL ethanol + 200 μL Nafion solution) was deposited onto the compact layer to form the Pt/(Nb-)TiO$_2$ electrode.

To determine the time constants for transfer of electrons from semiconductor (TiO$_2$, Nb-TiO$_2$, Pt/TiO$_2$, Pt/Nb-TiO$_2$) to the solution, we monitor the open-circuit potential decay (OCP) behaviors in the tri-electrode systems, in which 0.2 M PBS solution bubbled with argon or oxygen were used as the electrolyte (Figures S5, S6). Evaluating the time constants for interfacial transfer of electrons from (Nb-)TiO$_2$ to platinum cocatalyst can refer our recent publications.[3, 4]

To investigate the influence of sodium ions on the reduction half-reaction, the voltammetry behaviors of (Nb-)TiO$_2$ electrodes were characterized in the electrolyte with (0.1 M NaClO$_4$ + 0.4 M LiClO$_4$) and without (0.5 M LiClO$_4$) sodium salt (Figures 5, S11).

The photoinduced generation of hydroxyl radicals was characterized by dispersing 10 mg (Nb-)TiO$_2$ into 50 mL phosphate buffer solution (pH = 8.39) that contains 43 mM salicylic acid. Prior to irradiation, the system was bubbled with argon to remove dissolved oxygen. The

irradiation was provided by a 300-W high-pressure Hg-lamp. The generation rate of hydroxyl radicals was determined by measuring concentrations of 2,3-dihydroxybenzoic acid and 2,5-dihydroxybenzoic acid using a Hitachi high performance liquid chromatography (Figure S10).

To determine the influence of sodium ions on the hydroxyl radical generation, 10 mg Nb-TiO_2 were dispersed into salicylic acid solution that contains NaCl (5 g/L) or Na_2SO_4 (5 g/L). The concentrations of salicylic acid and the formed 2,3-dihydroxybenzoic acid and 2,5-dihydroxybenzoic were characterized by absorption spectroscopy (Figure S12).

The photoinduced adsorption of phenol was characterized by monitoring the bulk concentration of phenol. Firstly, 2 mL of (Nb-)TiO_2 slurry (formed by dispersing 1 g (Nb-)TiO_2 into 10 mL ethanol) were deposited onto the bottom of the reactor. After dried at room temperature, 30 mL phenol solution (20 μM) was introduced into the reactor. Prior to irradiation, the solution was bubbled with argon for 1 h. Then, the reactor was irradiated by a high-pressure Hg-lamp (63 mW/cm^2). To desorb the phenol from the (Nb-)TiO_2, 0.1 g KOH was introduced into the dispersion. The concentration of phenol in the bulk solution can be characterized by a Hitachi high performance liquid chromatography (Figure 1).

S3. Photocatalytic Mineralization. Photocatalytic mineralization of phenol was carried out in a fixed bed reactor equipped with a low-pressure mercury-lamp (PHILIPS, TUV, 30 W/G 30).[9] Firstly, 2 mL slurry formed by dispersing 1 g (Nb-)TiO_2 into 10 mL ethanol were coated on the surface of the mercury-lamp and dried naturally. The TiO_2 coated lamp was then placed into the reactor connected with a tank. The interspace of the reactor and the lamp was filled with 20 vol % methanol aqueous solution (200 mL containing 2 mg Pt in H_2PtCl_6 precursor) that was pumped from the tank. Platinum therefore can be deposited onto (Nb-)TiO_2 by photoinduced reduction.

Photocatalytic mineralization (Figures 4, S1, S8, S13) was performed by fluxing the phenol aqueous solution (42 mg/L × 1 L) with and without addition of NaCl (5000 mg/L) in the fixed bed reactor connected with a tank (Figure S14).[9, 10] During reaction, the phenol solution was bubbled with oxygen. Chemical oxygen demand (COD) values were monitored by sampling the phenol solution during the reaction with an interval of 0.5 h. The COD values were measured by a Water Quality analyzer (LH-T 725).
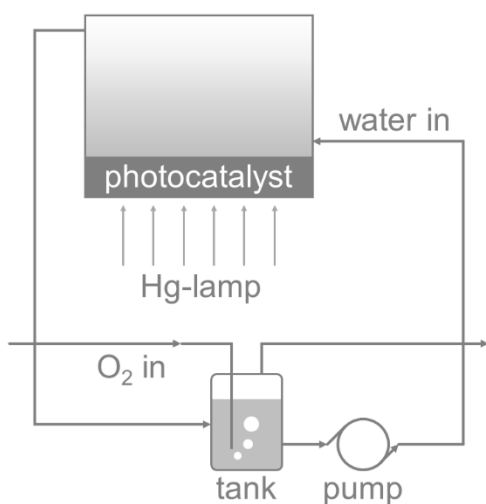

Figure S14. Schematic diagram of fixed bed reactor for photocatalytic contaminant mineralization.

Electronic Supplementary Information References

1.   Y. Fang, X. Wei, H. Liu, S. Gao, K. Jia, J. Wang and J. Chen, *Catal. Sci. Technol.*, 2023, **13**, 3495-3498.

2.   C.-H. Liao, S.-F. Kang and F.-A. Wu, *Chemosphere*, 2001, **44**, 1193-1200.

3.   X. Wei, S. Gao, H. Liu, Y. Fang and J. Chen, *J. Phys. Chem. Lett.*, 2023, **14**, 3721-3726.

4.   H. Xiang, Z. Wang and J. Chen, *J. Phys. Chem. Lett.*, 2021, **12**, 7665-7670.

5.   H. B. Tao, L. Fang, J. Chen, H. B. Yang, J. Gao, J. Miao, S. Chen and B. Liu, *J. Am. Chem. Soc.*, 2016, **138**, 9978-9985.

6.   H. Liu, X. Huang and J. Chen, *Chin. J. Catal.*, 2023, **51**, 49-54.

7.   R. A. Floyd, J. J. Watson and P. K. Wong, *J. Biochem. Biophys. Methods*, 1984, **10**, 221-235.

8.   E. Peralta, G. Roa, J. A. Hernandez-Servin, R. Romero, P. Balderas and R. Natividad, *Electrochim. Acta*, 2014, **129**, 137-141.

9.   X. Wei, H. Liu, S. Gao, K. Jia, Z. Wang and J. Chen, *J. Phys. Chem. Lett.*, 2022, **13**, 9642-9648.

10.   H. Xiang, Z. Wang and J. Chen, *Chin. J. Struct. Chem.*, 2022, **41**, 2209069-2209073.